DESIGN AND TESTING OF A GAS DISTRIBUTION METHOD FOR PULSED INDUCTIVE THRUSTERS

Except where reference is made to the work of others, the work described in this thesis is my own or was done in collaboration with my advisory committee. This thesis does not include proprietary or classified information.

_____

Robert E. Miller III

Certificate of Approval:

_____	_____
John Cochran Professor Aerospace Engineering	Roy J. Hartfield, Jr., Chair Professor Aerospace Engineering
_____	_____
Brian Thurow Assistant Professor Aerospace Engineering	Frank Rose Vice President of Research Radiance Technologies Inc.

_____

George T. Flowers
Dean
Graduate School

DESIGN AND TESTING OF A GAS DISTRIBUTION METHOD FOR PULSED INDUCTIVE THRUSTERS

Robert E. Miller III

A Thesis

Submitted to

the Graduate Faculty of

Auburn University

in Partial Fulfillment of the

Requirements for the

Degree of

Master of Science

Auburn, Alabama
December 19, 2008

DESIGN AND TESTING OF A GAS DISTRIBUTION METHOD FOR PULSED INDUCTIVE THRUSTERS

Robert E. Miller

_____
Signature of Author

_____
Date of Graduation

THESIS ABSTRACT

DESIGN AND TESTING OF A GAS DISTRIBUTION METHOD FOR PULSED INDUCTIVE THRUSTERS

Robert E. Miller III

Master of Science, December 19, 2008
(B.S., Auburn University, 1997)

64 Typed Pages

Directed by Roy Hartfield

A gas distribution manifold for use in a Pulsed Inductive Thruster has been designed and tested. The Argon test gas is distributed radially outward over a flat disc from an enclosed manifold area. The manifold was designed to meet a specific gas distribution time of one milli-second. Initial design of the manifold is determined from isentropic gas distribution assumptions. The manufactured prototype is tested at a vacuum background pressure of two to three milli-Torr. Gas distribution time for the flow over a simulated Pulsed Inductive Thruster surface is measured with respect to the manifold's exit using a modified form of Langmuir Probe. Error analysis for the measurement is provided. Measurement error range was less than 10% for all measurements.

ACKNOWLEDGEMENTS

The author would like to thank Radiance Technologies, and the Auburn University Space Research Institute for their support, patience and encouragement. Special thanks to Dr. Frank Rose, Zac Shotts, and Steve Best for guidance and assistance. Without their help, this project would not have been possible.

Style manual or journal used:	Modern Language Association Style Manual
Computer software used:	Microsoft Office Word 2003 Microsoft Office Excel 2003 UGS Solid Edge V19

TABLE OF CONTENTS

LIST OF TABLES

LIST OF FIGURES

NOMACLATURE

PIT	Pulsed Inductive Thruster
M(z)	Mutual Inductance (nH)
F	Force
L_c	Thruster coil unloaded inductance (nH)
z_o	Plasma decoupling distance (m)
z	Distance between the coil and plasma current
I_1	Current in the drive coil
I_2	Current in the plasma
I_{sp}	Specific Impulse (seconds)
m_{gas}	Mass of the gas above the disc at time of field trigger (Kg)
g	Gravitational constant equal to 9.8 m/s^2
C_r	Cross sectional area of individual channel
C	Capacitance (Farads)
V	Voltage (Volts)
η	Thrust Efficiency
P_{exit}	Manifold exit pressure (Pascals)
P_{init}	Static supply pressure (Pascals)
γ	Specific heat ratio
M_{exit}	Manifold exit Mach number
T_{exit}	Manifold exit Temperature (Kelvin)
T_{init}	Static supply Temperature (Kelvin)
ρ_{exit}	Density at the Manifold exit (Kg/m^3)
ρ_{init}	Static supply density (Kg/m^3)
u_{exit}	Manifold exit velocity (m/s)
a_{exit}	Speed of sound for the manifold exit temperature (m/s)
R_{Ar}	Gas constant for Argon equal to 208.1 J/(Kg-K)
$\dot{m}$	Mass flow rate (Kg/s)
CTA	Constant Temperature Anemometry
u_2	Velocity in the $\nu(M)$ direction (m/s)
v_r	Radial component of velocity (m/s)
r_{inner}	Magnetic coil disc inner radius (m)
r_{outer}	Magnetic coil disc outer radius (m)
μ	Viscosity of Argon
SNR	Signal to Noise Ratio
Std	Standard Deviation
Sm	Standard deviation of the mean

1. INTRODUCTION

1.1 Overview

A Pulsed Inductive Thruster (PIT) is a type of spacecraft electric propulsion that has been under research for over thirty years. Electrical energy is stored in a capacitor bank and then inductively discharged through flat, circular coil. A small amount, usually less than a tenth of a gram, of propellant is distributed over the coil in inert form prior to the electrical drive pulse. The gas is distributed over the coil in way that keeps it as close to the coil surface as possible. Gas is distributed from the center of the thruster from a manifold with a circumferential opening normal to the drive coil face. The gas is pulsed outward radially over the drive coil surface. The time of the gas distribution must be known such that the electrical pulse through the coil can be timed to the gas distribution. Upon initiation of the electrical pulse, the gas is first ionized either by the electrical drive pulse itself, or by a separate pre-ionization system. The ionized gas then couples to the magnetic field in the drive coil caused by the drive pulse. This induces a ring current parallel to the plane of the drive coil in the ionized propellant that is now a plasma. This now meets the requirement of a current carrying conductor (plasma) in a magnetic field, therefore force is applied to the plasma pushing it away from the drive coil. This applies an equal and opposite force on the drive coil, imparting an impulse thrust "bit" to the thruster.

Much of the early research and design work in the United States has been conducted by TRW, Inc. in conjunction with the Air Force Research Laboratories at Edwards Air Force base in California and later with NASA Glenn Research Center in Cleveland, Ohio. Current PIT related propulsion research is also being conducted in parallel by NASA at the Marshall Space Flight Center in Huntsville, Alabama in conjunction with the Institute for Scientific Research (ISR) Inc. and Radiance Technologies. This propulsion design has yet to be utilized in an operational spacecraft, but could potentially offer several advantages.[1, 2, 3] These advantages include:

1. Potential for low thruster specific mass (Kg/KW) as low as 15.6 Kg/KW[4] compared to other high power (≥ 10 KW), electric propulsion thruster designs under development.[5]
2. Capable of a wide range of average power levels in a single device.
3. Additional thrust control through throttled gas flow.
4. The PIT design will work with several propellant gases.
5. The PIT design is completely electrodeless. The design is therefore less susceptible to operational wear due to chemical reactions and sputtering than electric propulsion designs that require electrodes.[6]

PIT propulsion devices use a single pulsed magnetic field to first ionize the propellant gas and then accelerate the ionized propellant for thrust. The field coils used to create the magnetic pulse are integrated into a flat circular disc. The field coil geometry is shown on the right in Figure 1. The un-ionized propellant is initially dispersed over the disc. The disc and distribution manifold are shown on the left in

Figure 1. Then the magnetic pulse is timed to the gas distribution over the disc to achieve an optimum interaction between the magnetic field and the propellant.

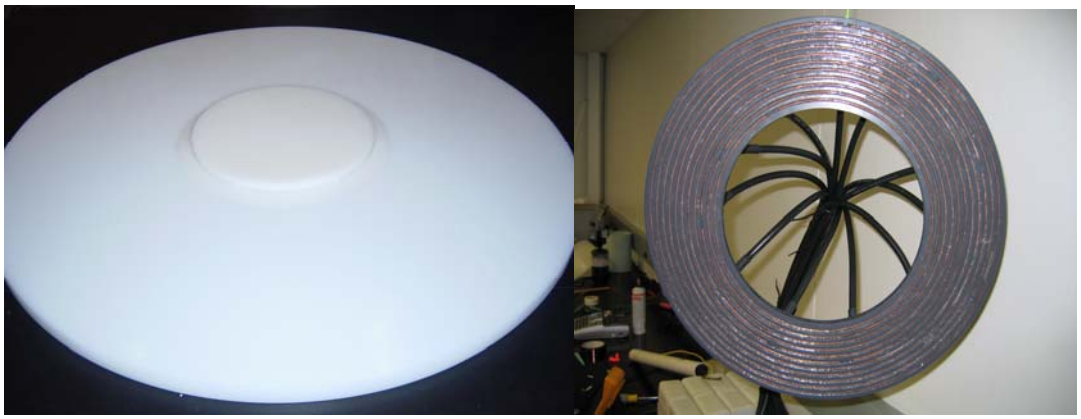

Figure 1: Geometry of the PIT and Field Coils Tested by Radiance

Optimization of the process requires that the propellant gas be as evenly distributed over the disc in the radial (r) and angular (theta) axes as possible with the gas as close to the disc as possible in the axial (z) direction. The cylindrical coordinate system is shown with respect to the device in Figure 2.

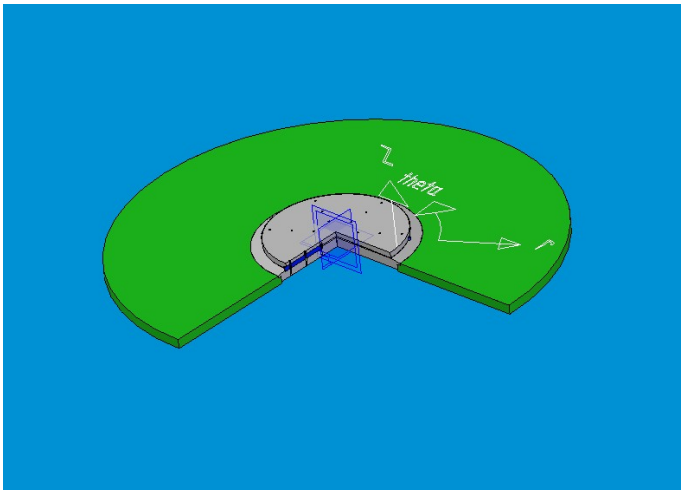

Figure 2: Cylindrical Coordinate System on the Disc

Ideally, there should be a uniform interaction between the pulsed magnetic field and the gas over the disc. This would lead to the best coupling efficiency between gas and magnetic field. When the electrical drive pulse and the ionized propellant interact, the coupling between the two currents is a function of the mutual inductance between the current in the drive coil, I_1, and the current ring, I_2, formed in the ionized propellant (plasma). The mutual inductance, given by eq. 1 is a function of unloaded coil inductance, L_o, the separation between the coil and the gas, z, and the plasma decoupling distance, z_o.[1] The plasma decoupling distance is a measure of the significant distance away from the coil at which the plasma becomes decoupled from the drive pulse. The force, F, generated due to the coupling between the two currents is given by eq. 2.

$$M = L_C \exp\left(\frac{-z}{z_o}\right) \tag{1}$$

$$F = -I_1 I_2 \frac{\partial M}{\partial z} = \frac{I_1 I_2 L_C}{2\, z_o} \exp\left(\frac{-z}{z_o}\right) \tag{2}$$

The physical shape, and therefore the coupling efficiency, of the plasma is determined by the uniformity and nearness of the initial inert gas distribution prior ionization to the drive coil at the start of the electrical drive pulse. If the gas is distributed near to the drive coil, well within the plasma decoupling distance, and in a uniform density, then the induced current, I_2, will be a maximum, and the greatest amount coupling distance, z_o, will be used for generated force during the plasma acceleration.

The amount of gas used and the magnitude of the magnetic field can be adjusted, such that a maximum fraction of the electrical energy in the magnetic field can be imparted into the propellant as directed kinetic energy in the positive z direction. If the

gas distribution is not uniform, then there will be a non-uniform coupling between gas and magnetic field. The amount of force generated by the acceleration of the plasma will be reduced.

The timing of the pulse for the field must also be coordinated to the gas distribution time for the same energy transfer reasons stated above. To coordinate the times, the distribution time of gas over the plate must be known and should be consistent. If the gas distribution time is a known constant, then onboard sensors will not be required to monitor the gas distribution to determine the trigger time of electromagnetic field pulse. It is also beneficial to make the distribution time as long as possible. For a given disc radius, this can be accomplished by keeping the radial distribution velocity of the gas as low as possible.

The gas is distributed over the disc in open space that is originally at vacuum levels of background pressure. The gas will achieve supersonic speeds for any distribution method chosen due to the low background pressure. The max velocity of the gas is given by eq. 3. The distribution time for the disc radius selected (~ 0.5 meters) will be roughly between 0.1 to 1.0 milliseconds for the supersonic gas velocity obtainable for Argon at a static gas temperature of 300 Kelvin and all drive coil and gas distribution manifold radii combinations of interest.

$$v_{\max} = \sqrt{2c_p T} \tag{3}$$

Achieving the slowest possible distribution time reduces the difficulty in timing the magnetic field pulse to the gas distribution. Also, if the distribution time is greater than or equal to one millisecond, then it might be possible that the pulsed power circuits

to the magnetic coils can be recharged fast enough to allow for near continuous gas supply and field pulses every one millisecond. This greatly increases the propellant utilization percentage since the gas leftover in the distribution system is not lost after every shot.

The design proposed in this thesis is one method to achieve the desired gas distribution time. The results of the work will show that the design lengthens the distribution time to around one millisecond. The uniformity of the gas distribution was not measured for this work, but could be measured at a later date using a Fast Ionization Gauge[1].

1.2 Historical Perspectives

1.2.1 United States Air Force

A one meter diameter PIT thruster was built and demonstrated by C.L. Bailey and R.H. Lovberg working for TRW Inc. under Air Force Research Laboratories contract during the 1970's.[1, 2, 3] This thruster preceded smaller devices (30 cm diameter) of the same design that were also tested. The TRW researchers found that the one meter thruster could generate a specific impulse of 2240 seconds whereas the smaller devices were limited to 1200 seconds. The conclusion was that the PIT design's efficiency increased with disc diameter. This was due to improved coupling between the ionizing gas and the pulsed magnetic field and therefore increased energy transfer. [1]

The TRW testing used a 20 μF capacitor bank charged to 20 KV to supply the voltage pulse to the field coils through a set of spark gaps. The sparks gaps were placed

in parallel in the circuit and triggered simultaneously. The design was sized to simulate a 25 Kilowatt mission. Testing yielded an overall efficiency of 50% thrust efficiency for this device. The efficiency is defined by eq. 4.[4]

$$\eta = \frac{\frac{1}{2} m_{gas} \left(g\, I_{sp}\right)^2}{\frac{1}{2} CV^2} = \frac{Kinetic\ energy\ produced}{Electical\ energy\ in} \tag{4}$$

The gas distribution system used a radial, supersonic nozzle placed at the center of the disc. The nozzle was mounted on a pylon several centimeters high. The gas was fed to the nozzle under high pressure by a fast acting valve that provides a 150 microsecond gas pulse in a single pulse operational mode. The gas pulse fed to the supersonic nozzle was directed downward in the z direction and also expanded radially outward toward the plate by the nozzle. This gas pulse exited the nozzle at approximately MACH 2.0. The magnetic field pulse was then timed to coincide with the time at which the gas pulse would be nearest the disc. [1]

The gas distribution for the design used in the TRW work was measured with a fast ionization gauge. A Schlieren system was also used with limited success due to the low gas distribution pressure.[3] The TRW researchers found that a significant percentage of the propellant gas could be compressed into a reflected shock wave near the disc face.

Losses still existed in this distribution design for three reasons. First, some of the gas would radially expand past the edge of the disc, and was therefore not utilized as propellant. Second, some of the gas was not contained in the shock wave near the plate, and was present above the disc at a height at which it could not interact with the magnetic field. A portion of the gas was therefore not accelerated by the magnetic field, but

entrained by gas that did interact with the field. This leads to a lower overall I_{sp}, and a reduction in efficiency. Third, this design employed a much higher gas density near the center pylon, with the gas density decaying exponentially radially. This resulted in an uneven gas distribution profile across the disc with respect the radial direction, reducing the effective ability to couple the magnetic field to the gas propellant.[3]

The magnetic field timing window required to effectively take advantage of the gas distribution produced by this design is less than one microsecond in breadth. This requires a very accurate means to time the magnetic field pulse to the gas distribution with very little room for timing error. In addition, due to the high z velocity component of the gas during distribution, the compressed shock wave spends less than four microseconds in a band below a reasonably useable height for interaction with the magnetic field. Therefore, the magnetic field pulse used with this system should be compressed down to no more than three to four microseconds in pulse width to effectively couple with the gas before the gas moves outside effective range.

1.2.2 NASA

During the past decade NASA has been working with the TRW one meter diameter PIT thruster at the Glenn Research Center at Cleveland, Ohio. This effort entails attempting to replace the spark gaps switches with solid state devices, and operational testing of the thruster at high repetition rate to evaluate its performance. The power supply for this testing is a 250 KJ capacitor bank that can supply 30 Megawatts for two milliseconds.

The effort also includes an attempt to model the plasma formation and acceleration using the MACH2 code. The magneto hydrodynamics MACH2 model is a time-dependent, two-dimensional, axis-symmetric, multi-material code based upon a time-advanced finite-volume spatial differencing method. The model treats the gas as a compressible, viscous fluid.[6] These efforts are in concert with other electric propulsion research in an attempt to develop a high-power electric thruster. [7]

In 2004 research into alternative technology application for the pulsed inductive thruster design began at Radiance Technologies. These studies included the application of a Vector Inversion Generator to replace the capacitor bank, pre-ionization of the propellant gas, and simplification of the magnetic field design and pulse delivery mechanism. The design and testing described in this thesis was also conducted under this contract.

The basic goal of this work was to provide a gas distribution system for use in PIT that would distribute the gas close to the thruster in a known amount of time. The desired distribution time should be more than 1 millisecond. This would allow the thruster to be operated in a burst rep-rate mode at a 1 Khz rep-rate. By operating in this mode, the thruster could work with a slower gas valve, since the pulse time of the valve would be determined by the time duration of the burst, and not the time duration of the individual pulse. A radial distribution of the gas was chosen since this should keep the gas close to the thruster face. The gas distribution was not measured for this work. Experimental focus was on the gas pulse distribution time.

2. METHODOLOGY

The design considerations outlined in the introduction provided the starting point for design of the gas distribution manifold. In order to simplify the solution, the flow was approximated as steady state. If the flow is considered steady state, then the isentropic nozzle equations can be used to characterize the gas velocity. The flow is a gas pulse, and is therefore inherently dynamic. The starting background pressure inside the manifold is at vacuum. Prior to establishing a steady state pressure distribution inside the manifold the gas would be under-expanded and would therefore accelerate to above the speed of sound inside the nozzle. The exit of the manifold becomes the choke point of the flow after the steady state pressure distribution inside the nozzle is established. The results of the testing will show that the approximation of the flow as steady state did predict the measured distribution times with an accuracy suitable for practical design purposes. A CAD model of the manifold is shown in figure 3.

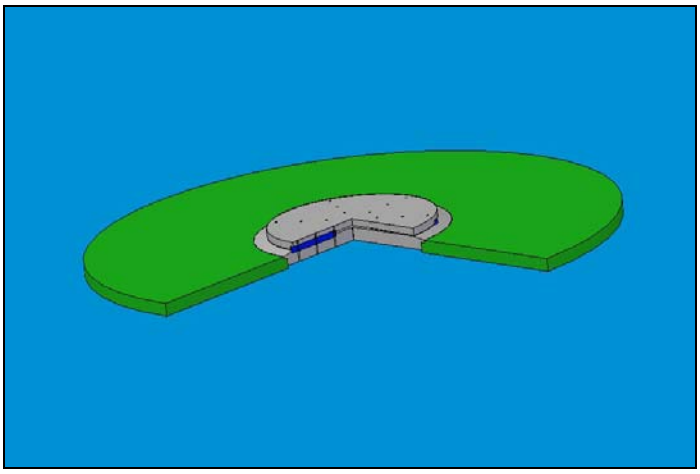

Figure 3: Cross Sectional Cutaway of the Gas Distribution System and Disc

If the flow were unsteady inside the manifold, the expected gas velocity would reach the speed of sound prior to exiting the nozzle. For Argon at a static temperature of 300 K the speed of sound is 322.9 m/s. During experimental measurement of the flow, the time that it takes the flow to go through the manifold was measured to 0.97 milliseconds by the modified Langmuir method that will be described later in the thesis. The length of the flow path through the manifold is 0.18 meters. The average speed of the flow in the manifold is given by eq. 5.

$$V_{avg} = \frac{flow\ path\ length}{time} = \frac{0.18\ meters}{0.97 \times 10^{-3}\ \text{sec}} = 185.6\ m/s \qquad (5)$$

In the steady state condition, the flow accelerates from approximately zero velocity in the radial (r) direction to Mach one at the manifold exit. The average subsonic velocity calculated based upon the measured travel time is evidence that the flow is either near or at steady state conditions. If the flow were not near steady state, a sonic or supersonic average velocity would be more likely.

The design chosen constrains the geometry of the enclosed portions of the device to ensure that the exit point of the gas (from the manifold) is a convergent nozzle for a steady state flow. The manifold is pictured in Figures 4 through 6. The exit is the smallest cross sectional area encountered by the gas during distribution. The gas will accelerate to supersonic speeds over the plate due to free expansion. However, the gas starts this expansion from the lowest speed possible for the given negligible background pressure, which is Mach one, set by the convergent nozzle geometry. This ensures that the speed of the gas will be as low as possible during distribution over the disc for a maximum distribution time.

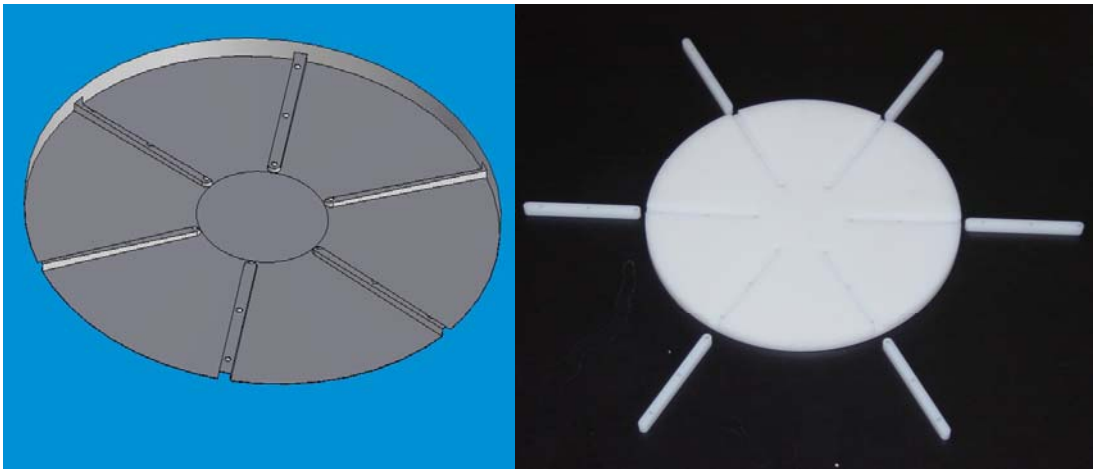

Figure 4: Manifold Internals Part A

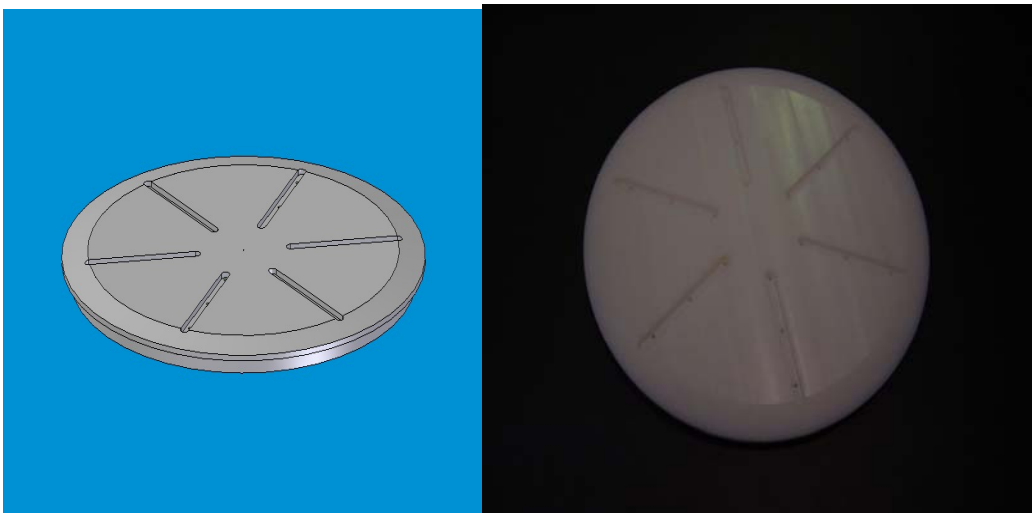

Figure 5: Manifold Internals Part B

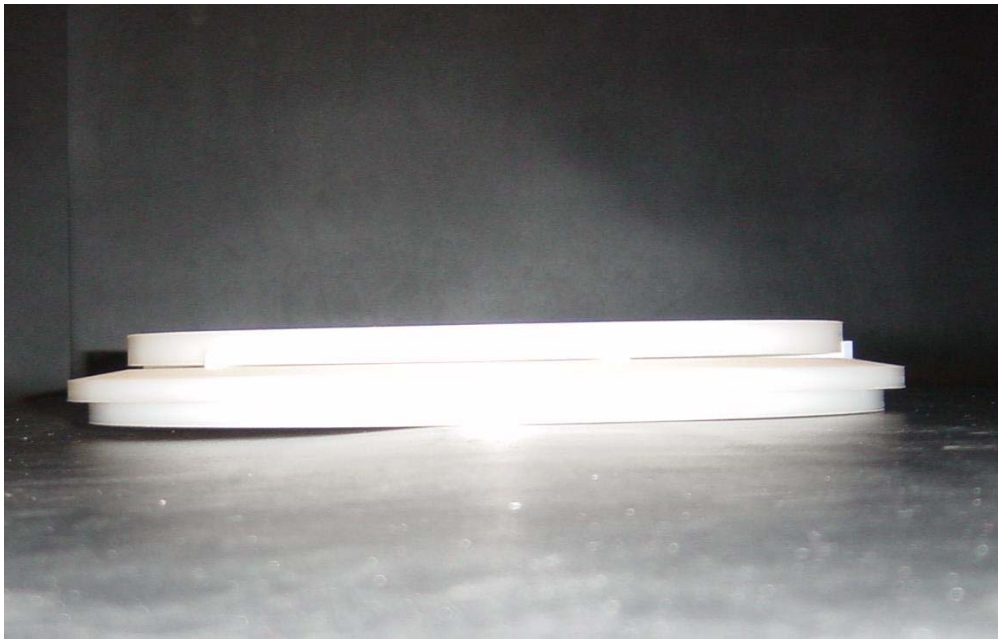

Figure 6: Nozzle Exit Side View

2.1 Gas Distribution Time Measurement (Overview)

Ultra Heavy Molecular Weight (UHMW) polypropylene was selected as the material due to its ease in milling. The full assembly with the manifold and disc are pictured in Figure 1.

The device was placed into a vacuum chamber on a test stand. Constant Temperature Anemometry (CTA) was the first attempted means to measure the gas distribution time. The gas density proved too low to make CTA a viable measurement tool. A technique utilizing a modified form of Langmuir probe[8] was developed to detect the passage of the gas. A Langmuir probe is a form of electrical plasma instrumentation that is typical used to measure plasma electron temperature and plasma ion density. For further information on this system, please see ref. 8. Two such instruments were used to monitor for passage of the gas. One probe was placed at the exit of the manifold and the other at the edge of the plate. Therefore, the time difference between the trigger points of the two detectors would be the distribution time. The sensor setup is shown in Figure 7.

The distribution time of the gas, as measured would then provide a rough estimate of the best time to trigger the magnetic field pulse. The flow across the plate is a pulse instead of steady state for pulsed operation of the thruster. For pulsed operation, the optimum gas distribution may occur over a relatively small amount of time (with respect to the distribution time) before or after the initial front of the gas pulse has passed. Therefore, the optimum trigger time would likely be some time near but not exactly equal to the distribution time. This optimum time could be identified on a fully operational thruster by varying the magnetic field pulse time in small increments in the time range

slightly past the time when the initial gas front reaches the edge of the disc. The thrust could be measured for the different trigger times of the magnetic field pulse until an optimum trigger time could be found.

In a continuous gas supply thruster design the gas supply is not pulsed for each shot. The optimum time for the magnetic field pulse trigger in this design would likely be coincident with the distribution time. Since the flow is steady state for this design consideration, the optimum achievable gas distribution is likely that predicted by the model.

2.2 Choice of test gas

Argon was chosen as the gas to be used for testing of the device. The PIT design will work with several types of gases; however, Argon has several advantages for testing. Argon is monatomic therefore; its specific heat ratio is a constant for a large temperature range. Argon is easily ionized, readily available for testing purposes, safe to handle, and remains a gas at relatively low temperatures. Helium has many of the same properties as Argon, but has a higher gas speed. This would result in a faster distribution time for Helium as compared to Argon.

Argon is easily ionized and its Paschen curve has been well characterized.[9] This simplified the calibration of the probes since the applied voltages were chosen such as to trigger ionization with a minor change in Argon gas pressure. The sensitivity of the probes was on the order of one milli-Torr increase in Argon gas pressure above the starting two to three milli-Torr background pressure.

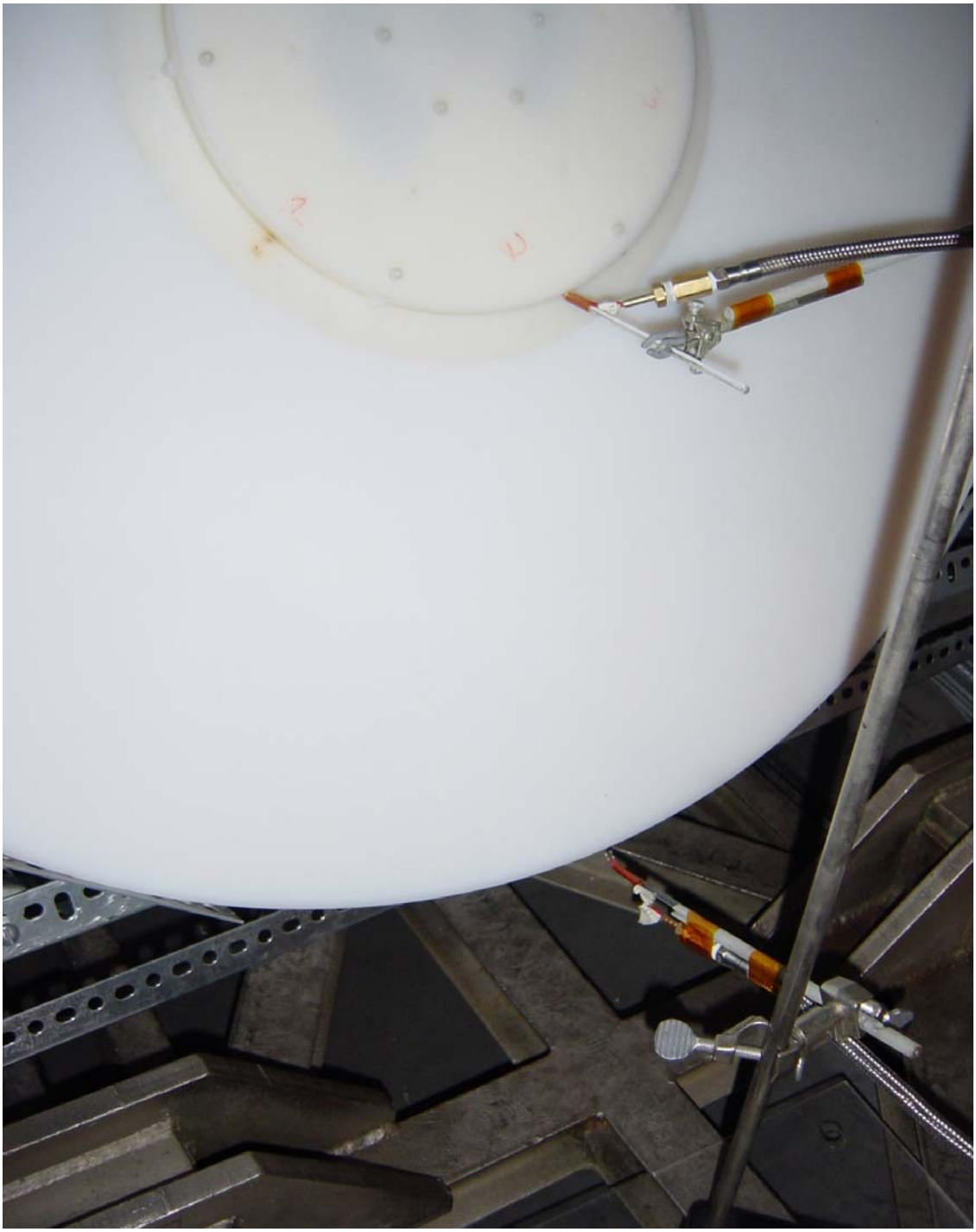

Figure 7: Testing Setup in the Vacuum Chamber

3. THEORY

All aspects of the design and testing are presented in this section in detail. The gas distribution is divided into two main areas. The first area presented is the flow of gas through the internal area of the manifold. Distribution over the disc is then discussed. The section concludes with a description of the testing instrumentation and setup.

3.1 Internal flow through the distribution system

The flow path for the gas starts at the center of the manifold shown in Figure 3. It is delivered by a pulsed solenoid valve supplied by a relatively constant pressure Reservoir. The gas expands radially outward in six equal areas defined by the ribs, between the two halves of the manifold. Each area of expansion has a slightly decreasing cross sectional area as the gas moves outward in the radial direction. This was accomplished by narrowing the distance between the upper and lower halves of the manifold as a function of the manifold's radius. The internal portions of the gas distribution system, or manifold are shown in figures 8 and 9.

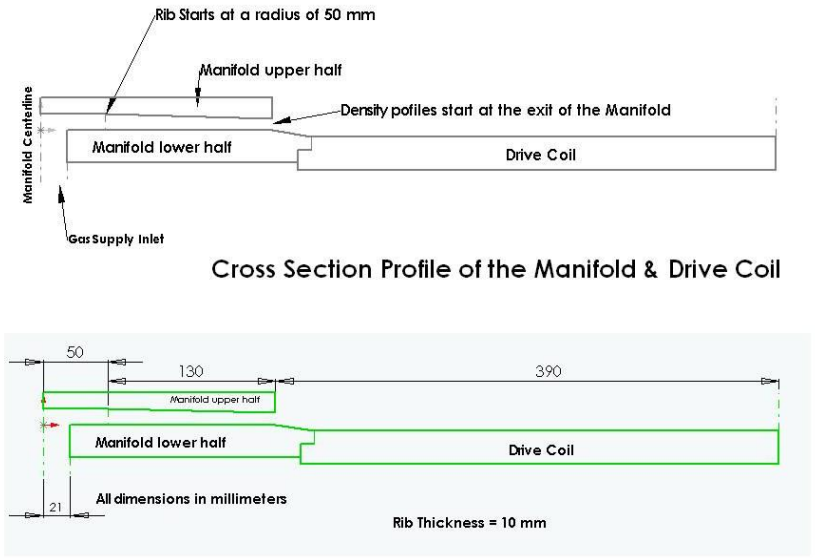

Figure 8: Diagram Cutaway of the Gas Distribution System and Disc

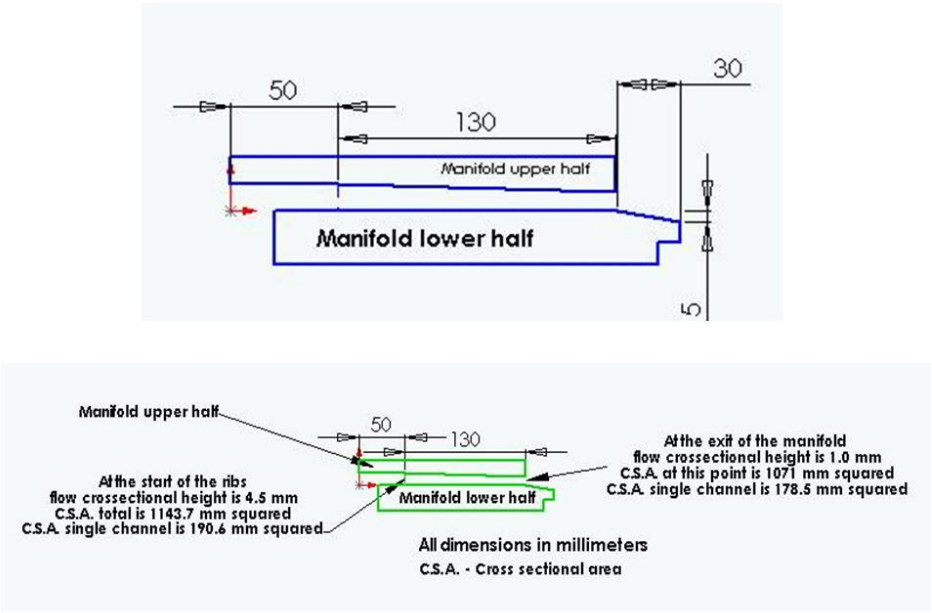

Figure 9: Control of the crossectional area by varying height

The initial radius, where the ribs begin to divide the flow into six separate channels is 50 mm. The cross sectional area, C_r, for each of these six flow areas corresponding to this radius is given by eq. 6.

$$C_r = \frac{1}{6}\left(2\pi Radius - rib\ thickness\ x\ 6\right)\left(height\right) \tag{6}$$

The rib thickness is 10 mm. The height between the plates at radius of 50 mm is 4.5 mm. This provides a cross sectional area of 190.6 mm^2 for each of the six flow areas. The total cross sectional area at this radius is 6 x 190.6 mm^2 = 1143.7 mm^2. The outer radius of the enclosed flow area is 180.0 mm. The height between the plates at this point is 1.0 mm. This results in a cross sectional flow area for each of the six areas of 178.5 mm^2 at the outer edge of the manifold. The total cross sectional area at this radius is 6 x 178.5 mm^2 = 1071.0 mm^2.

Since the cross sectional area at the outer edge of the plate is maintained slightly smaller than for all radial cross sections on the interior of the manifold, this outer edge becomes the nozzle throat. The geometry established is that of a converging nozzle. Therefore, the maximum velocity that can be obtained within the internal area of the manifold is Mach one for steady flow. This is the assumed speed at the throat of the nozzle, where the flow becomes choked.

The flow exits the manifold at Mach one, which is the lowest Mach number attainable for steady flow in any nozzle geometry, given that the flow is under expanded. An under expanded flow being one in which the exit pressure of the flow is greater than that of the exit surroundings.[10] For steady flow under these conditions, the throat is guaranteed to have a choked flow condition. The Mach number at the throat will be

Mach one. (Since the manifold deposits the gas into a vacuum, the flow will always be under expanded.)

The gas properties at the exit of the manifold can be approximated from the steady isentropic nozzle equations. For the purpose of this analysis the Mach number at the exit of the manifold is fixed at one, and γ for Argon is a fixed number equal to 1.67. The steady isentropic nozzle equations are presented in eqs. 7 through 9.[10]

$$P_{exit} = P_{init}\left(1 + \frac{\gamma - 1}{2} M_{exit}^{\ 2}\right)^{\frac{-\gamma}{\gamma - 1}} \tag{7}$$

$$T_{exit} = T_{init}\left(1 + \frac{\gamma - 1}{2} M_{exit}^{\ 2}\right)^{-1} \tag{8}$$

$$\rho_{exit} = \rho_{init}\left(1 + \frac{\gamma - 1}{2} M_{exit}^{\ 2}\right)^{\frac{-1}{\gamma - 1}} \tag{9}$$

These equations can be reduced to simpler statements for Argon exiting the manifold as shown in eqs. 10 through 12.

$$P_{exit} = 0.49\ P_{init} \tag{10}$$

$$T_{exit} = 0.75\ T_{init} \tag{11}$$

$$\rho_{exit} = 0.65\ \rho_{init} \tag{12}$$

The velocity at the exit of the manifold is then given by eq. 13.

$$u_{exit} = M_{exit} a_{exit} = M_{exit}\sqrt{\gamma R_{Ar} T_{exit}} \tag{13}$$

The method for determining the mass flow rate at the exit of the nozzle is dependent upon the delivery method. The delivery method can be split into two distinct

categories. The gas could be delivered either from a relatively small measured volume (constant volume source) or from a supply line or large reservoir (constant pressure source). The first method would be the most likely method to use for a pulse over a short time frame. The second method would be the most likely method for a continuous gas supply. The continuous gas supply scheme would require delivery from a supply line (constant pressure source) since a measured volume for this scheme would be impractically large. In addition, the constant volume would not be able to provide a constant mass flow rate due to large pressure drop over time, a problem inherent to the constant volume source.

Regardless of supply scheme, a fast acting valve with a cross sectional area larger than the total cross sectional area at the manifold exit would be required at the entrance of the manifold for future designs. A poppet type or diaphragm type valve would be appropriate for this application. This would ensure that amount of gas wasted (not on the disc at time of magnetic field pulse) would be minimized and that the manifold exit cross sectional area would remain the choke point for the gas flow.

A slower acting poppet type valve was used for the purpose of testing. The cross sectional area of the valve is larger than one of the six sections of the manifold. Of the six sections on the manifold, all but one was sealed off for measurement of the flow times. The solenoid operated, poppet type supply valve was placed outside the vacuum chamber to simplify design of the gas supply system. This resulted in a long leg of supply piping joining the supply valve and the manifold. The amount of gas wasted per pulse was not a consideration for this stage of design and testing, since the sole purpose

of the experimental setup was to measure the flow time over the disc. The additional length of piping did not prove to be an inhibiting factor to the testing.

The gas was supplied to the poppet valve by a large gas reservoir that experienced less than a 1% change in static, supply pressure per shot. Since the pressure change in the reservoir per shot was minimal, it could reasonably be considered a constant pressure source. This reservoir is larger than would be reasonable for use on a flight ready thruster due to space and weight considerations.

The mass flow rate equation for a steady state constant pressure source method using a nozzle is given by eq. 14.

$$\dot{m} = \frac{AP_{init}\sqrt{\gamma}}{\sqrt{R_{Ar}T_{init}}} M\left(1+\frac{\gamma-1}{2}M^2\right)^{-\frac{\gamma+1}{2(\gamma-1)}} \tag{14}$$

The choked nozzle exit design factor requires that the manifold exit remain the point at which the flow is choked to control mass flow rate. This places a constraint on the gas supply system, in that the supply line prior to entry to the manifold must have a cross sectional area greater than the combined cross sectional area for the manifold exit. The manifold's combined cross sectional area at the exit is given in eq. 15.

$$\begin{aligned} &Exit\ cross\ \text{sec}tional\ area_{comb} = \\ &\qquad 6\ x\ 178.5\ mm^2 = 1071\ mm^2 = 1.071\ x\ 10^{-3}\ m^2 = 1.66\ in^2 \end{aligned} \tag{15}$$

This corresponds to a radius of 18.46 mm or 0.727 inches for a circular pipe. Therefore, the supply line prior to entry to the manifold, where the static conditions are measured, must be greater than or equal to this radius in size. For testing purposes, this constraint was impractical due the necessity to feed the gas into the vacuum chamber through a bulkhead fitting. This fitting was slightly smaller than the required radius. To

alleviate this constraint, all but one the six sections in the manifold were closed off from flow. This was done through the application of duct seal, a putty material, to inlet of these areas. This ensured the desired flow geometry was maintained.

The desired mass distributed across the disc is 1 x 10^{-5} kg . The mass bit size was selected based upon prior work by Loveberg and Dailey on pulsed inductive thrusters of this diameter.[1] The desired distribution time is one millisecond. The resulting design mass flow rate is 1 x 10^{-2} kg/s. A supply temperature of 300 K is assumed. The isentropic equations for flow through a convergent nozzle are presented in eqs. 7 through 14 for the required supply pressure. Note that viscous effects on the supply gas inside the distribution system are ignored. Substituting in the values for geometry, gas properties and Mach number gives eq. 16.

$$P_{init} = 3208\ Pa = 3.208\ KPa \tag{16}$$

The equation can also be solved as a function of temperature;

$$P_{init} = 104.2\sqrt{T_{init}} \tag{17}$$

The supply temperature cannot practically be much less than 300 K to ensure that the propellant, Argon, does not reach its critical temperature of 151 K inside the manifold and subsequently interfere with the gas distribution over the disc. The lower supply temperature limit to prevent this is 202 K.

The following factors have not been taken into account in the design and were considered to be relatively unimportant for preliminary design purposes here;

1. The time dependence of the flow field governing eqs.
2. Frictional heating of the gas in the manifold

3. Heat transfer between the manifold and disc components and the gas flow
4. Possibility of temporal flow instabilities internal to the manifold
5. Turbulence
6. Flow interaction with the disc during expansion over the disc

3.2 Testing Method

The testing phase of this project focused primarily on determining the gas distribution time across the plate. Initial attempts to measure density distribution were conducted using constant temperature anemometers. This method proved unsuccessful and a method using gas detection through gas ionization was pursued as an alternate method. This alternate method proved successful in measuring the gas distribution time.

3.2.1 Modified Application of Dual Langmuir Probes

After failure of the CTA probes, it was suggested by Auburn Space Research Institute Lab Manager Steve Best that given the extremely low operating background pressures of the manifold the gas flow could possibly be ionized under high voltage potential. This basic concept is used by Dual Langmuir Probes which are often used to study low density plasmas.[9] The electrical characteristics of the gas medium (Argon in this case) are described by the Paschen curve shown in figure 10.[9]

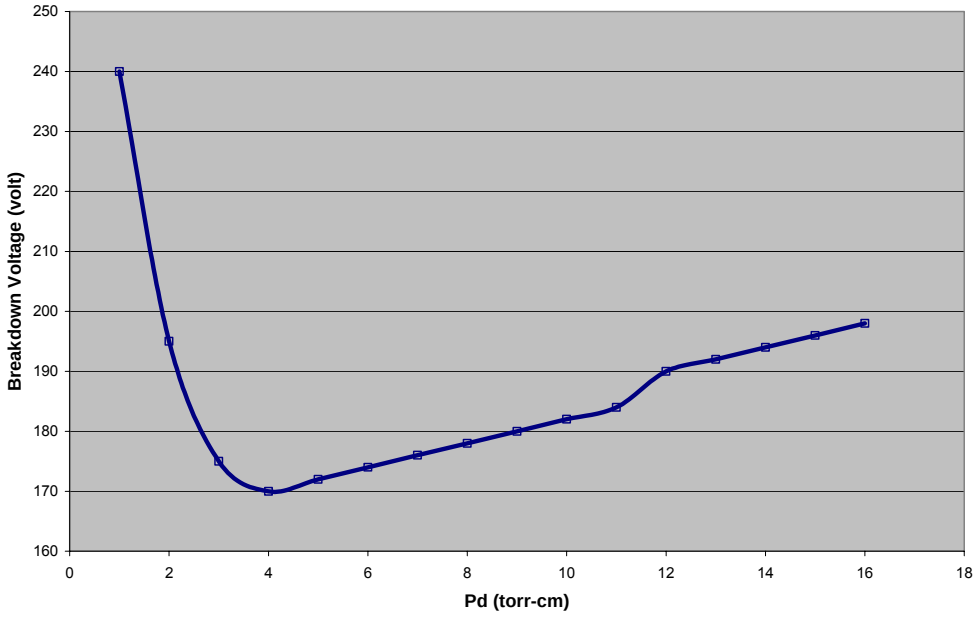

Figure 10: Paschen curve for Argon

The Paschen curve predicts the conditions under which the Argon gas will ionize taking into account the applicable dimension of the probe – lead separation. The curve provides the threshold voltage across the sensor leads required to ionize the Argon gas versus the compound parameter of gas pressure multiplied by the probe lead separation. The operational range of interest for this measurement falls to the far left side of the Paschen curve. For regions of very low pressure (in the milliTorr range) found in the present investigation, the curve is nearly vertical. Therefore, a sensor separation of one to three millimeters will allow for a high resolution of pressure change detection. The sensors used had a lead separation distance of 2.0 mm. This lead separation was found to work best in practice.

Initial testing proved this application to be viable. Negatively biased DC voltage potential just low enough to not cause discharge (gas ionization) without gas flow was applied. When the gas was pulsed through the manifold, passing the point where the probe was placed, ionization occurred and a detectable signal was produced. The sensor described was connected to a circuit that provides a capacitive voltage of three to six kVDC negatively biased potential to the sensor. The Voltage level is set such that the sensor will not trigger at background pressure, but will trigger with a pressure increase of one to three milli-Torr overall at the probe location. Starting background pressure in the vacuum chamber was established between two to three milli-Torr for each measurement. When the sensor is triggered by the gas, a path is established to discharge the capacitor across the sensor leads. The voltage potential for the capacitor of each sensor was monitored by oscilloscope. An electrical schematic for a single channel of the sensor system is provided in Figure 11.

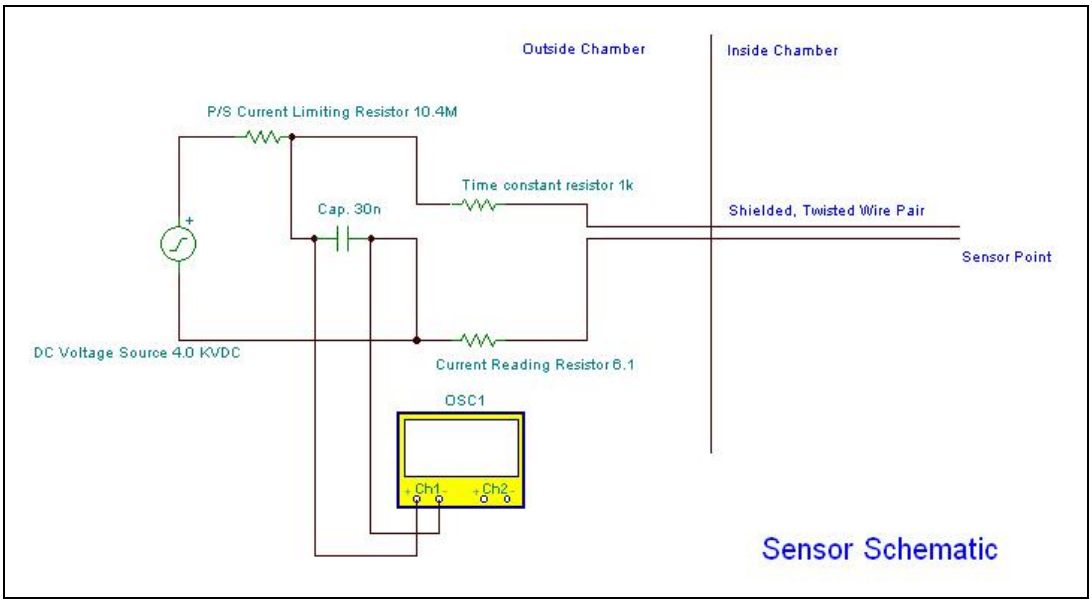

Figure 11: Sensor Schematic

An initial attempt to use this sensor for gas distribution time utilized two independent sensors of the design described above. The first one placed at the manifold exit and the second placed at the outer edge of the PIT disc. The RF signal generated by the firing of the first sensor was large enough to trigger the second sensor. To prevent this effect, the sensor lines required electrical shielding up to and as close as possible to the probe leads for all connecting wiring inside the vacuum chamber.

It was also determined that sharp edges on the probe leads created a field geometry that was not conducive to this application. Distribution times measured with probe leads of this type were very random. To overcome this problem, the probe leads were made tear-drop shaped through the application of solder, such that no sharp edges were left on the leads. The final configuration of the sensor leads is shown in Figure 12.

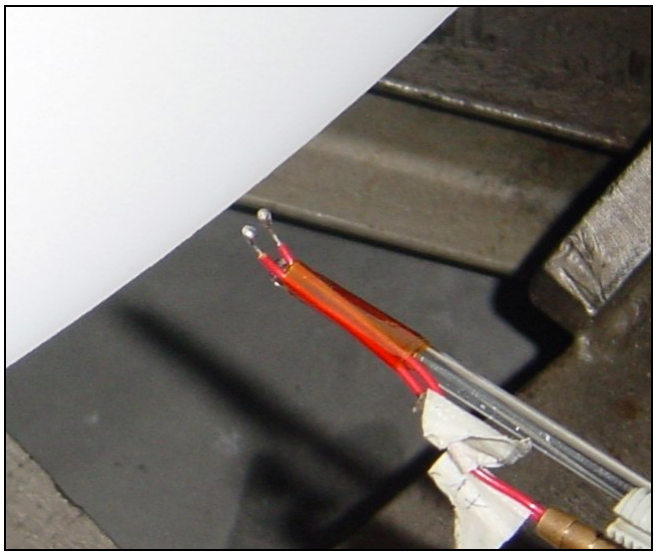

Figure 12: Close-up View of a Sensor

3.2.2 Verification of the Modified Dual Langmuir Probes

With the sensor design established, the next step was to test their operation. The manifold and PIT simulation disc were removed from the chamber leaving only the gas supply line. A third monitor point for the oscilloscope was added. This point was the voltage supply for the solenoid valve used to supply the gas pulse. The solenoid valve is shown in Figure 13. The power supply for the solenoid valve was a capacitor bank, whose voltage drop upon valve pulse initiation could be consistently used to mark the start of the gas pulse. An electrical schematic for the solenoid valve's pulsed power supply is provided in Figure 14.

Since the oscilloscope's initial trigger point was independent of the sensors, any deviation in the distribution time could be isolated to one or the other sensors. The measurement method using the third time point was used for all measurements including those taken on the disc after sensor validation.

Figure 13: Solenoid Used to Pulse Gas to the Manifold

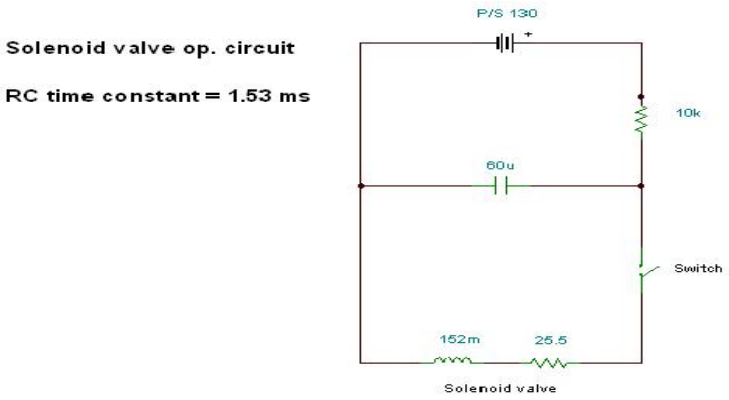

Figure 14: Solenoid Valve Operation Circuit

The exit cross sectional area of the supply line was reduced such that the exit became a choked nozzle for the supply line. One sensor was placed at the nozzle exit and the second was placed 390 millimeters directly out in front of the nozzle. To verify the

sensors, five different test runs were executed. Each of the five tests included at least ten data points. The data presented in Tables 1 through 5 represents the time at which the sensors triggered after the initiation of the gas pulse at the solenoid valve by the application of the electrical pulse from the capacitor bank. The time difference between the trigger points for the two sensors is the distribution time, or travel time, for the gas between the two sensors. All time measurements are in milliseconds.

Three of the tests used the same nozzle exit cross sectional area of 197.9 mm^2. This area was calculated to be small enough to provide choked nozzle exit geometry for supply line. The first two tests compare alternate sensor orientations with respect to the gas flow. One run was conducted with the sensors oriented perpendicular to the gas flow. This data is presented in Table 1. The second run (Table 2) was conducted with the sensor oriented parallel to the gas flow. This was done to show that trigger time of the sensors was independent of sensor orientation to the gas flow. The distribution time for both orientations was the same within measurement error. The distribution time for each of these runs agreed with the predicted distribution time within one standard deviation for both data sets. Note that the standard deviation of the mean, Sm, is given for all data sets by eq. 18 as a function of the standard deviation, Std, and n, the number of data points in the test set.

$$S_m = \frac{Std}{\sqrt{n}} \tag{18}$$

During the third test run with a nozzle exit cross sectional area of 197.9 mm^2, the supply pressure was increased. The data for this test is presented in Table 3. This was done to verify that the nozzle exit was choked. Since the distribution time measured for

this test did not vary from the two lower supply pressure runs, it provides verification that the nozzle was indeed choked.

As a comparison, if the gas distribution time is estimated considering the Mach number to be constant at a value of one over the entire disc, then the distribution time is 1.4 milliseconds. If the gas distribution time is estimated considering the Mach number to be constant at a value of two over the entire disc, the distribution time is 0.93 ms.

Table 1: Choked Test Nozzle Data Perpendicular Sensor Orientation

Choked test nozzle ($197.9\ mm^2$) with a sensor separation of 390 mm, 10 PSIA of supply pressure and sensors oriented perpendicular to the gas flow. All data in milliseconds		
Sensor 2 trigger time	Sensor 1 trigger time	distribution time
10.84	9.92	0.92
10.84	9.96	0.88
11.12	10.36	0.76
11.28	10.20	1.08
11.00	9.96	1.04
10.84	9.92	0.92
11.20	10.00	1.20
11.04	9.76	1.28
10.88	9.84	1.04
11.04	9.96	1.08
average	average	average
11.01	**9.99**	**1.02**
standard deviation of the mean	standard deviation of the mean	standard deviation of the mean
0.05	0.05	0.05

Table 2: Choked Test Nozzle Data Parallel Sensor Orientation

Choked test nozzle ($197.9\ mm^2$) with a sensor separation of 390 mm, 10 PSIA of supply pressure and sensors oriented parallel to the gas flow. All data in milliseconds		
Sensor 2 trigger time	Sensor 1 trigger time	distribution time
10.80	9.96	0.84
11.56	10.28	1.28
11.60	10.16	1.44
11.28	10.04	1.24
10.96	10.00	0.96
11.28	9.92	1.36
10.84	9.96	0.88
11.28	9.88	1.40
11.20	9.80	1.40
10.52	9.76	0.76
average	average	average
11.13	**9.98**	**1.16**
standard deviation of the mean	standard deviation of the mean	standard deviation of the mean
0.11	0.05	0.08

Table 3: Choked Test Nozzle Data Increased Supply Pressure

Choked test nozzle ($197.9\ mm^2$) with a sensor separation of 390 mm, 14 PSIA of supply pressure and sensors oriented perpendicular to the gas flow. All data in milliseconds		
Sensor 2 trigger time	Sensor 1 trigger time	distribution time
10.72	9.76	0.96
10.64	9.72	0.92
10.64	9.80	0.84
10.32	9.80	0.52
10.68	9.76	0.92
10.68	9.76	0.92
10.84	9.76	1.08
10.96	9.72	1.24
11.08	9.72	1.36
10.76	9.76	1.00
average	average	average
10.73	**9.76**	**0.98**
standard deviation of the mean	standard deviation of the mean	standard deviation of the mean
0.06	0.01	0.07

For the fourth test, the cross sectional area of the choked nozzle was reduced to 112.4 mm^2. The same distribution time was measured within one standard deviation for the data as for the larger, but still choked nozzles and the computer simulation prediction time. This data is presented in Table 4.

Table 4: Reduced Area Choked Test Nozzle Data

Choked test nozzle (112.4 mm^2) with a sensor separation of 390 mm, 10 PSIA of supply pressure and sensors oriented perpendicular to the gas flow. All data in milliseconds		
Sensor 2 trigger time	Sensor 1 trigger time	distribution time
10.88	10.12	0.76
11.68	10.04	1.64
10.60	10.00	0.60
11.16	10.00	1.16
11.08	9.96	1.12
11.52	9.96	1.56
11.52	9.96	1.56
10.92	9.88	1.04
11.04	9.88	1.16
10.72	9.88	0.84
10.60	9.84	0.76
average	average	average
11.07	**9.96**	**1.11**
standard deviation of the mean	standard deviation of the mean	standard deviation of the mean
0.11	0.02	0.11

For the fifth test, the nozzle exit cross sectional area was increased to 357.5 mm^2. This area was calculated to be large enough to provide convergent – divergent nozzle geometry for the distribution system exit. Therefore, the exit velocity from the nozzle would be supersonic and the distribution time would be shorter. The distribution time was estimated as follows. The exit cross sectional area of 357.5 mm^2 provides an area ratio of 1.81 for the given supply piping diameter. From this area ratio, the initial Mach number was determined to be 2.25. Since the supply temperature is 300K (relatively

low), the distance of concern is relatively small (0.39 meters) and the initial Mach number was high, then the change in velocity for the expanding velocity is relatively small. Based upon these assumptions, the distribution time was predicted to be approximately 0.8 milliseconds using the Mach 2.25 exit velocity condition. The measured distribution time did concur with this estimated time as shown in Table 5.

Table 5: Supersonic Test Nozzle Data

Supersonic test nozzle (357.5 mm^2) with a sensor separation of 390 mm, 10 PSIA of supply pressure and sensors oriented perpendicular to the gas flow. All data in milliseconds		
Sensor 2 trigger time	Sensor 1 trigger time	distribution time
10.72	10.12	0.60
10.84	10.08	0.76
10.64	10.00	0.64
10.64	9.84	0.80
10.56	9.80	0.76
10.64	9.88	0.76
10.64	9.84	0.80
10.72	9.80	0.92
10.96	9.92	1.04
10.52	9.80	0.72
average	average	average
10.69	**9.91**	**0.78**
standard deviation of the mean	standard deviation of the mean	standard deviation of the mean
0.04	0.04	0.04

The sensor's trigger time is dependent upon lead separation, gas pressure, and applied voltage. This behavior as discussed is characterized by the Paschen curve for the gas used, which in this case is Argon. The operational region chosen for the sensor is in an area where the Paschen curve is nearly vertical. In this region, the gas ionization threshold is on the order of a few milli-Torr in pressure difference. The pressure contacting the sensors from the gas pulse for this testing was several orders of magnitude

larger than this threshold. The sensors' response time is therefore several orders of magnitude smaller than the characteristic time scale, and its response to the gas passage reliable. Overall, the accuracy range of the instrument appears to be reasonable, based upon the standard deviation of the mean showing the repeatability of the measurements and the correlation of the measured flow times to the expected values based upon calculated flow properties.

3.2.3 Difficulties in Use of the Modified Dual Langmuir Probes

It is noted that the sensors do experience an anomalous behavior after approximately fifteen gas pulses. After approximately this number of pulses, it was repeatedly observed that the second sensor would take several milliseconds longer to trigger than previous readings. This would occur for two to three pulses and then the sensor would not respond at all. To restore operation, the vacuum chamber would be re-pressurized to atmospheric pressure and then pumped back down to an initial test pressure of two to three milli-Torr. After the pressure cycling of the chamber, the sensor would return to normal operation for approximately another fifteen pulses. This behavior occurred without fail for every test run.

The cause of this behavior could not be determined, but is believed not to be indicative of the gas distribution. The longer time responses just prior to sensor failure were disregarded. The sensors were operated taking into account this behavior with the vacuum chamber pressure cycled as necessary to restore sensor operation.

In addition to the above anomalous behavior, the sensors also proved to be temperamental in operation. The problems experienced with the sensors ranged from a failure to trigger at all to erratic readings. The erratic readings included trigger times that indicated impossibly short or impossibly long distribution times. In any instance that the readings became erratic with widely varying readings, the test run was terminated. The entire experimental setup was inspected for problems and the test run was repeated. If erratic readings continued, then the sensor leads were rebuilt. In every case during which erratic readings were experienced, normal operation of the sensors could be restored. Since the erratic readings could be cleared by rebuilding the sensors and no other change in the experimental setup, it is reasonable to believe that the behavior was due solely to sensor malfunction and not attributable to the gas distribution.

4. RESULTS AND ERROR ANALYSIS

4.1 Experimental Data

After verifying the operation of the sensor system the PIT disc and manifold were reinstalled into the vacuum chamber as shown in Figure 6. The sensors were placed such that the first sensor was at the manifold exit and the second was at the edge of the disc. At the edge of the PIT simulation disc (radius of (180+390) mm), measurements were taken at heights (distance perpendicular off the disc face) of 3 mm, 5 mm, 10 mm, 15 mm, 30 mm, 45 mm, and 60 mm.

A single testing point at 50% of the distribution length, 195 mm, and a height of 5 mm was also studied. The results of this test run are presented in Table 13. More test points at 25%, 50%, and 75% disc length were planned, but unfortunately the vacuum chamber experienced technical difficulties that prevented further testing. All of the data collected is presented in Tables 6 through 13.

Table 6: Test Data for Edge of the Disc and Height of 3 mm

Cumulative data for the point at the disc edge at a height of 3 mm above the disc surface. All data in milliseconds		
Sensor 2 trigger time	Sensor 1 trigger time	Distribution time (S_2 time – S_1 time)
11.96	10.92	1.04
12.20	10.96	1.24
11.84	11.08	0.76
12.12	11.04	1.08
12.24	11.00	1.24
11.92	10.92	1.00
11.88	10.96	0.92
11.64	10.92	0.72
12.00	10.84	1.16
12.60	11.24	1.36
12.28	11.08	1.20
12.28	11.08	1.20
11.84	11.12	0.72
12.72	11.12	1.60
12.48	11.04	1.44
12.04	11.04	1.00
11.88	11.04	0.84
11.88	10.92	0.96
12.28	10.84	1.44
12.20	11.24	0.96
11.72	11.08	0.64
11.88	11.00	0.88
12.24	11.00	1.24
11.68	10.80	0.88
12.84	10.96	1.88
average	average	average
12.11	**11.01**	**1.10**
standard deviation of the mean	standard deviation of the mean	standard deviation of the mean
0.06	0.02	0.06

Table 7: Test Data for Edge of the Disc and Height of 5 mm

Cumulative data for the point at the disc edge at a height of 5 mm above the disc surface. All data in milliseconds		
Sensor 2 trigger time	Sensor 1 trigger time	Distribution time (S_2 time – S_1 time)
12.12	11.08	1.04
12.24	10.96	1.28
12.48	11.00	1.48
11.84	11.04	0.80
12.12	11.12	1.00
12.08	11.00	1.08
12.32	10.88	1.44
11.88	10.92	0.96
11.96	10.92	1.04
11.44	10.88	0.56
11.88	10.92	0.96
12.24	10.92	1.32
11.84	10.92	0.92
11.92	10.92	1.00
11.84	10.88	0.96
12.00	10.96	1.04
12.48	10.88	1.60
11.96	10.96	1.00
12.04	10.84	1.20
12.24	10.72	1.52
11.52	10.88	0.64
11.96	10.84	1.12
12.52	11.04	1.48
12.44	10.92	1.52
12.28	10.88	1.40
12.16	10.84	1.32
11.36	10.84	0.52
11.68	10.80	0.88
11.96	10.76	1.20
11.48	10.68	0.80
12.08	10.68	1.40
11.40	10.72	0.68
11.64	10.52	1.12
11.48	10.72	0.76
12.16	10.68	1.48
11.52	10.60	0.92
11.88	10.72	1.16
11.88	10.76	1.12
11.32	10.56	0.76
average	average	average
11.94	**10.85**	**1.09**
standard deviation of the mean	standard deviation of the mean	standard deviation of the mean
0.05	0.02	0.05

Table 8: Test Data for Edge of the Disc and Height of 10 mm

Cumulative data for the point at the disc edge at a height of 10 mm above the disc surface. All data in milliseconds		
Sensor 2 trigger time	Sensor 1 trigger time	Distribution time (S_2 time – S_1 time)
12.24	11.08	1.16
11.84	10.96	0.88
12.32	10.88	1.44
12.80	10.92	1.88
11.84	10.84	1.00
11.96	10.60	1.36
11.76	10.68	1.08
12.04	10.68	1.36
12.28	10.72	1.56
12.12	10.76	1.36
11.64	10.92	0.72
11.84	10.76	1.08
11.72	10.64	1.08
11.20	10.60	0.60
11.76	10.56	1.20
12.00	10.72	1.28
12.08	10.72	1.36
11.48	10.68	0.80
11.64	10.76	0.88
12.76	10.72	2.04
average	average	average
11.97	**10.76**	**1.21**
standard deviation of the mean	standard deviation of the mean	standard deviation of the mean
0.09	0.03	0.08

Table 9: Test Data for Edge of the Disc and Height of 15 mm

Cumulative data for the point at the disc edge at a height of 15 mm above the disc surface. All data in milliseconds		
Sensor 2 trigger time	Sensor 1 trigger time	Distribution time (S_2 time – S_1 time)
12.12	11.04	1.08
12.00	11.08	0.92
12.16	11.00	1.16
11.72	11.00	0.72
11.80	11.00	0.80
12.00	10.96	1.04
12.20	11.04	1.16
12.72	11.16	1.56
11.64	10.96	0.68
11.48	10.88	0.60
12.32	10.96	1.36
11.68	10.88	0.80
12.40	10.96	1.44
12.40	10.84	1.56
12.56	11.00	1.56
12.36	10.88	1.48
12.04	10.96	1.08
12.40	11.04	1.36
12.08	11.00	1.08
11.60	11.00	0.60
11.88	11.08	0.80
11.96	11.04	0.92
11.68	10.88	0.80
11.68	11.00	0.68
11.72	10.84	0.88
12.32	10.72	1.60
11.64	10.68	0.96
11.36	10.48	0.88
12.24	10.60	1.64
11.24	10.44	0.80
average	average	average
11.98	**10.91**	**1.07**
standard deviation of the mean	standard deviation of the mean	standard deviation of the mean
0.07	0.03	0.06

Table 10: Test Data for Edge of the Disc and Height of 30 mm

Cumulative data for the point at the disc edge at a height of 30 mm above the disc surface. All data in milliseconds		
Sensor 2 trigger time	Sensor 1 trigger time	Distribution time (S_2 time – S_1 time)
12.04	11.12	0.92
12.12	11.04	1.08
12.72	11.16	1.56
11.84	11.08	0.76
12.08	10.96	1.12
12.16	11.04	1.12
12.40	11.40	1.00
11.68	11.00	0.68
11.80	10.80	1.00
11.64	10.92	0.72
12.04	11.12	0.92
11.96	10.88	1.08
11.96	10.96	1.00
11.76	10.92	0.84
11.96	10.88	1.08
11.68	10.92	0.76
12.64	11.00	1.64
12.68	10.96	1.72
12.76	11.36	1.40
12.32	11.20	1.12
11.72	10.96	0.76
11.60	10.92	0.68
12.40	11.04	1.36
12.00	10.88	1.12
11.52	10.76	0.76
11.76	10.76	1.00
11.92	10.68	1.24
12.08	10.68	1.40
average	average	average
12.04	**10.98**	**1.07**
standard deviation of the mean	standard deviation of the mean	standard deviation of the mean
0.07	0.03	0.06

Table 11: Test Data for Edge of the Disc and Height of 45 mm

Cumulative data for the point at the disc edge at a height of 45 mm above the disc surface. All data in milliseconds		
Sensor 2 trigger time	Sensor 1 trigger time	Distribution time (S_2 time – S_1 time)
11.84	10.88	0.96
12.20	10.84	1.36
11.72	11.04	0.68
11.96	10.84	1.12
12.12	10.80	1.32
11.52	10.72	0.80
11.88	11.12	0.76
12.68	10.72	1.96
12.32	10.64	1.68
11.96	10.64	1.32
12.04	11.04	1.00
12.08	10.80	1.28
11.56	10.76	0.80
11.92	10.72	1.20
11.72	10.80	0.92
11.68	10.64	1.04
12.36	10.76	1.60
11.76	10.88	0.88
12.40	11.00	1.40
12.00	10.92	1.08
average	average	average
11.99	**10.83**	**1.16**
standard deviation of the mean	standard deviation of the mean	standard deviation of the mean
0.07	0.03	0.08

Table 12: Test Data for Edge of the Disc and Height of 60 mm

Cumulative data for the point at the disc edge at a height of 60 mm above the disc surface. All data in milliseconds		
Sensor 2 trigger time	Sensor 1 trigger time	Distribution time (S_2 time – S_1 time)
12.56	11.44	1.12
11.72	11.00	0.72
11.44	10.80	0.64
12.56	10.68	1.88
11.64	10.88	0.76
12.20	10.84	1.36
11.96	10.84	1.12
11.96	10.96	1.00
11.60	10.80	0.80
12.04	10.68	1.36
12.16	11.16	1.00
12.00	10.68	1.32
12.36	10.68	1.68
12.44	11.08	1.36
11.72	10.60	1.12
12.12	10.76	1.36
average	average	average
12.03	**10.87**	**1.16**
standard deviation of the mean	standard deviation of the mean	standard deviation of the mean
0.09	0.06	0.09

Table 13: Test Data for 50% of the Disc Length and Height of 5 mm

Cumulative data for the point 195 mm from the manifold exit (50% length) at a height of 5 mm above the disc surface. All data in milliseconds		
Sensor 2 trigger time	Sensor 1 trigger time	Distribution time (S_2 time – S_1 time)
11.60	11.00	0.60
11.24	10.88	0.36
11.40	11.16	0.24
11.84	11.16	0.68
11.44	11.04	0.40
11.96	11.44	0.52
11.60	11.16	0.44
11.56	11.08	0.48
11.52	11.16	0.36
11.76	11.16	0.60
11.40	10.72	0.68
11.64	11.24	0.40
11.64	11.20	0.44
11.52	11.00	0.52
11.72	11.04	0.68
11.52	11.04	0.48
11.52	10.88	0.64
11.48	10.88	0.60
11.44	10.88	0.56
11.16	10.76	0.40
11.36	10.84	0.52
average	average	average
11.54	**11.03**	**0.50**
standard deviation of the mean	standard deviation of the mean	standard deviation of the mean
0.04	0.04	0.03

Table 14: Summary of the Test Results for Measurements Taken at Disc Edge

Summary of testing for all data taken at the edge of the disc - distance of 390 mm. All data in milliseconds		
Height above the disc	Measured distribution time	Standard deviation of the mean
3 mm	1.10	0.06
5 mm	1.09	0.05
10 mm	1.21	0.08
15 mm	1.07	0.06
30 mm	1.07	0.06
45 mm	1.16	0.08
60 mm	1.16	0.09

A summary of the average gas distribution time measurements for various heights, z, is given in table 14. These measurements show that the gas distribution time is slightly greater than one millisecond, and that the manifold does fulfill this aspect of the design criteria. If further studies were done to study the density distribution over the drive coil, this data could contribute to understanding the flow properties overall. However, no data other than the distribution time is available at this time, there are no further conclusions about the flow characteristics that can be made from these few data points.

In addition to the data collected on the distribution time across the disc it can also be said that the average time the gas spends in the manifold is 0.97 milliseconds. This is based upon the difference between the cumulative time average for the time to the manifold entrance from the solenoid valve and the time to the manifold exit from the solenoid valve. The time through the gas supply piping downstream of the solenoid

valve to the manifold entrance was taken from the average of the cumulative sensor one readings during the sensor verification testing.

This measurement can be used for this purpose since the supply piping remained unchanged throughout the testing. The time required for the gas to transit through both the supply piping and the manifold together can be determined from the sensor one data with the manifold and disc in place. The difference between the two averaged time readings gives the estimate (0.97 milliseconds) of the gas distribution time through the manifold alone.

4.2 Error Analysis

The standard deviation for all test measurements is presented with the data in Tables 1 through 13. The standard deviation of the mean, σ, provides a measurement of the data spread. For any single test run, given the average value of the measurement, x, there is a 68% probability that the actual value of x lies within the range of $x \pm \sigma$. There is a 96% probability that the actual value of measurement lies within the range of $x \pm 2\sigma$. The average distribution time and standard deviation of the mean for the average distribution time for all the measurements taken with the manifold in place is summarized in Table 15 and 16. For each reading the data range corresponding to the probability range is presented. Also, as a metric, the percentage variation of average distribution time that this range corresponds to is presented.

Table 15: Summary of the Standard Deviation for all test data 68% probability range

Test Run (by data table number)	exp. measured avg. distribution time (ms)	Standard Deviation (σ)	68% probability	
			x±σ range (ms)	±% avg reading
table 1	1.02	0.05	(0.97,1.07)	5%
table 2	1.16	0.08	(1.08,1.24)	7%
table 3	0.98	0.07	(0.91,1.05)	7%
table 4	1.11	0.11	(1.00,1.22)	10%
table 5	0.76	0.04	(0.72,0.80)	5%
table 6	1.1	0.06	(1.04,1.16)	5%
table 7	1.09	0.05	(1.04,1.14)	5%
table 8	1.21	0.08	(1.13,1.29)	7%
table 9	1.07	0.06	(1.01,1.13)	6%
table 10	1.07	0.06	(1.01,1.13)	6%
table 11	1.16	0.08	(1.08,1.24)	7%
table 12	1.16	0.09	(1.07,1.25)	8%
table 13	0.5	0.03	(0.47,0.53)	6%

Table 16: Summary of the Standard Deviation for all test data 96% probability range

Test Run (by data table number)	exp. measured avg. distribution time (ms)	Standard Deviation (σ)	96% probability	
			x±2σ range (ms)	±% avg reading
table 1	1.02	0.05	(0.92,1.12)	10%
table 2	1.16	0.08	(1.00,1.32)	14%
table 3	0.98	0.07	(0.84,1.12)	14%
table 4	1.11	0.11	(0.89,1.33)	20%
table 5	0.76	0.04	(0.68,0.84)	11%
table 6	1.1	0.06	(0.98,1.22)	11%
table 7	1.09	0.05	(0.99,1.19)	9%
table 8	1.21	0.08	(1.05,1.37)	13%
table 9	1.07	0.06	(0.95,1.19)	11%
table 10	1.07	0.06	(0.95,1.19)	11%
table 11	1.16	0.08	(1.00,1.32)	14%
table 12	1.16	0.09	(0.98,1.34)	16%
table 13	0.5	0.03	(0.44,0.56)	12%

Table 15 indicates that there is a 68% probability that the actual average distribution time for any single test run is within ± 6% (on average) of the measured

average value. Table 16 indicates that there is a 96% probability that the actual average distribution time for any single test run is within ± 13% (on average) of the measured average value.

Additional experimental measurements with more precise sensors should be made to determine the gas distribution over the thruster. The time limit for the contract under which the research contained in this thesis was conducted expired prior to conducting additional testing. Additional testing is planned in conjunction with future work.

5. CONCLUSION AND RECOMMENDATIONS

The testing results for distribution time across the thruster showed that the gas is distributed in the desired time range. Due to time constraints, an improved gas distribution measurement method was not employed at this time. Additional measurements of the density distribution should be made to show that the distribution of the gas is adequately close to the thruster surface to ensure magnetic coupling to the thruster's pulsed magnetic field.

Given that is takes 0.97 milliseconds for the gas to pass through the manifold compared to 1.06 milliseconds for it to travel over the PIT disc two recommendations can be made. First, as dimensioned, this manifold would work well for a continuous gas supply PIT, but not for a single pulse PIT. In a single pulse engine a large percentage of the gas would be wasted in the manifold not utilized on the disc. If this manifold design were planned to be used with a PIT that would have partial duty as a pulsed unit, then I would recommend shortening the radius of the manifold and the disc proportionately. This would reduce the overall percentage of gas wasted in the manifold in a single pulse operational mode.

The knowledge and experience gained during the research conducted by ISR and Radiance Technologies will be harnessed on a new electric propulsion project under the

direction of the NASA Marshall Space Flight Center in Huntsville, AL. This new research will focus on a similar electric propulsion design, the Faraday Accelerator with Radio-frequency Assisted Discharge (FARAD). The electric propulsion design works the same way that the PIT does, except the propellant is pre-ionized prior to acceleration by the electromagnetic field. A RF antenna that requires little energy when compared to the acceleration field pulse pre-ionizes the gas. Therefore, the acceleration field pulse is not partially expended performing this function prior to accelerating the propellant. This increases the efficiency of the engine since a larger fraction of the acceleration field pulse can be then used to accelerate the propellant.[11]

The manifold design work conducted in this thesis will be incorporated into the FARAD project. The FARAD thruster designed will be 30 cm in diameter, instead of the1 meter diameter used for the PIT project. The manifold design will be scaled down to fit the 30 cm diameter thruster design.

REFERENCES

1. Dailey, C.L. and Lovberg, R.H., "Large Diameter Inductive Plasma Thrusters", AIAA paper 79-2093, Princeton/AIAA/DGLR 14th International Electric Propulsion Conference, Princeton, New Jersey, October 1979.

2. Dailey, C.L., "Pulsed Electromagnetic Thruster", Technical Report AFRPL-TR-71-107, Air Force Rocket Propulsion Laboratory, Edwards Air Force Base, California, December 1971.

3. Dailey, C.L. and Lovberg, R.H., "Large Inductive Thruster Performance Measurement", AIAA paper 81-0708R, American Institute of Aeronautics and Astronautics Journal, Vol. 20, No. 7, July 1982.

4. Dailey, C.L. and Lovberg, R.H., "Experimental Data for a One-Meter Diameter Pulsed Inductive Plasma Thruster with Application to a 25 KW mission", unpublished.

5. Martinez-Sanchez, M. and Pollard, J.E., "Spacecraft Electric Propulsion – An Overview", Journal of Propulsion and Power, Vol. 14, No. 5, 1998, pp. 688 – 699.

6. Mikellides, Pavlos G., "Pulsed Inductive Thruster (PIT): Modeling and Validation Using the MACH2 Code", NASA/CR-2003-212714, NASA Glenn Research Center, Chelveland, Ohio, 2003.

7. NASA Glenn Research Center, "2001 Research and Technology", NASA/TM-2002-211333, NASA Glenn Research Center, Chelveland, Ohio, March 2002.

8. Hopkins, M.B., "Langmuir Probe Measurements in the Gaseous Electronics Conference RF Reference Cell", J. Res. Natl. Stand. Technol. 100, 415, Journal of Research of the National Institute of Standards and Technology, Vol. 100, No. 4, July-August 1995.

9. Petraconi, G., et al., "Longitudinal Magnetic Field Effect on the Electrical Breakdown in Low Pressure Gases", Brazilian Journal of Physics, Vol. 34, No. 4B, December, 2004

10. Anderson, John D., Modern Compressible Flow With Historical Perspective, McGraw Hill, New York (2004)

11. Polzin, Kurt Alexander, *Faraday Accelerator with Radio-frequency Assisted Discharge (FARAD),* Ph.D. Dissertation, Dept. of Mechanical and Aerospace Engineering, Thesis No. 3147-T , Princeton Univ., Princeton, NJ, 2006.